Journal of Magnetics 11(2), 77-82 (2006)

Increment of the Exchange Coupling in Fe-Ni Alloy Thin Films Deposited with a Bias Magnetic Field

Kyung Hunn Han[1]*, Jung Gi Kim[2], Jae Hun Cho[3], and Sukmock Lee[3]

[1]*Proton Engineering Frontier Project, Korea Atomic Energy Research Institute, Daejeon 305-600, Korea*
[2]*Department of Physics, Hanyang University, Seoul 133-791, Korea*
[3]*Department of Physics, Inha University, Incheon 402-751, Korea*

(Received 19 December 2005)

The structure and magnetic properties of Fe-Ni films, deposited by DC magnetron sputtering on Si(111) wafer, have been studied. The spin wave stiffness constant is determined by Brillouin light scattering (BLS) and compared with the value obtained from magnetization measurements. The range of exchange interaction was determined as 0.4 atomic distances in the film deposited in a bias magnetic field, which is 1/2 that in the film grown in no bias magnetic field. The results show that the dimensions of exchange coupling increased by the sputtering in the magnetic field.

Key words : brillouin light scattering, soft magnetic film, Fe-Ni alloy, spin wave stiffness, exchange interaction

1. Introduction

Iron-Nickel is one of the most intensively investigated 3d metallic alloys. In part, the property of magnetic moment of $Fe_{1-x}Ni_x$ alloys($x \geq 0.65$) with the fcc structure shows an anomalous behavior with substantial deviations from the Slater-Pauling curve [1]. Numerous theoretical explanations have been put forward to account for the Invar Phenomenon such as low thermal expansion properties [2]. On the other hand, the spin-wave dispersion relation in the ferromagnetic Invar alloys has been investigated using the neutron scattering [3], spin wave resonance [4], and magnetization measurements [5, 6] in the past few decades. It has been suggested from experimental results that the SW stiffness constant D has a minimum near the $x = 0.4$ due to the origin of the instability of the ferromagnetism in the Invar region [7]. It has long been known that in the fcc phase of Fe-Ni alloys the Fe-Fe magnetic coupling could be antiferromagnetic for small Fe-Fe nearest-neighbor distance [8].

The purpose of the present study is to understand experimentally the changes in the magnetic properties for Fe-Ni films deposited with and without additional constant bias magnetic field (H_{bias}). The choice of experimental method to determine the spin wave (SW) stiffness constant is the Brillouin light scattering (BLS) [9] and magnetization measurements. In this work, we report on the magnetic properties of the Fe-Ni alloy and particularly on the difference in the SW stiffness constants by the effect of bias magnetic field.

*Corresponding author: Tel: +82-42-868-2882,
e-mail: khhan178@kaeri.re.kr

2. Experiment

DC magnetron sputtering was used in sample fabrication. A hybrid target consisting of Ni chips placed on Fe disc with the purity of 99.99% covering 9.9% of the disc surface was used as a target. The size of deposit plane is approximately 8 mm in diameter on a Si(111) of square-type of 10×10 mm [9]. The base pressure was 3×10^{-7} Torr or better. The dc power and the substrate temperature were maintained at 50 W and 250 °C, respectively, during deposition. The total pressure of Ar gas during the sputtering is fixed at 1 mTorr. The distance between the substrate and target is kept at 80 mm. During deposition an additional constant bias field of 500 Oe is applied parallel to the plane of the film in order to introduce uniaxial anisotropy. The films grown without and with an applied bias magnetic field are labeled FZ and FG respectively. The thickness of these films was measured using a profilemeter. The crystal structure was confirmed using X-ray diffraction with *Cu-Kα* radiation

in θ-2θ geometry. The wavelength, accelerating voltage, and current are 1.5418 Å, 40 kV, and 40 mA, respectively. The film composition is deduced from Energy Dispersive X-ray Spectrometer (EDS). Magnetic properties were measured by vibrating sample magnetometer (VSM) with a maximum magnetic field of 100 Oe at room temperature. Spin waves were studied by a Sandercock (3+3) multipass tandem Fabry-Perot interferometer [10]. The probe light source used is a single longitudinal mode of 514.5 nm line of an Argon ion laser with output power of about 300 mW. Backscattering geometry is used to observe the light scattered by thermal excitations with an in-plane wavenumber $q_{//} = 1.727 \times 10^5$ cm^{-1} with the angle of incidence as 45.

3. Result and Discussion

The crystal structure of the films is confirmed by XRD. Figure 1 gives the XRD patterns for the FZ and FG samples with the thickness of 40 nm and 100 nm, respectively. The results of XRD show that the films have a pure fcc crystal structure. As shown in Fig. 1, the relative position of diffraction peaks for the (200) plane for FG samples is shifted about 0.3 degree from those for FZ samples. These positions are related to the lattice constant. The values obtained for lattice constant are summarized in Table 1. the lattice constants of FG samples show larger values than those of the FZ samples. The grain sizes are calculated from the XRD line broadening of the (111) and (200) peak, using the classical Scherrer relationship [11], $D_{hkl} = k\lambda/B\cos\theta$, where D_{hkl} is the grain diameter in nm, k is a constant (shape factor) with a value of 0.9, B is the half-maximum line width, and λ is the X-ray wavelength. The obtained values for grain sizes are summarized in Table 1. As seen in Table 1, the grain size is dependent on the various deposition conditions.

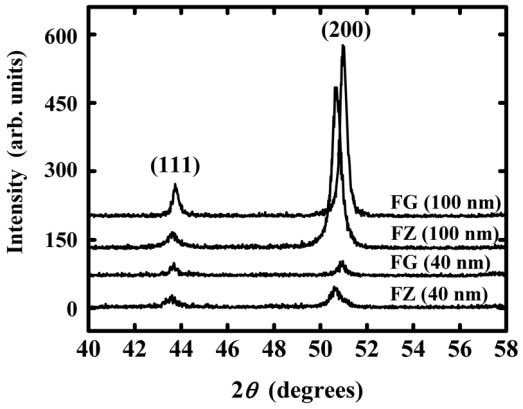

Fig. 1. XRD patterns for the FZ and FG samples with different thickness.

Table 1. Grain sizes and lattice constant obtained by XRD patterns of Fig. 1. And chemical composition of the FZ and FG samples.

Deposition condition	Thickness [nm]	XRD Grain size (111) peak [nm]	XRD Grain size (200) peak [nm]	XRD Lattice constant [Å]	EDS Atomic% Fe	EDS Atomic% Ni
FZ	40	15.66	15.7	3.62	59.26	40.74
	100	17.62	20.18	3.64	57.18	41.82
FG	40	24.94	22.39	3.57	55.16	44.84
	100	29.08	26.79	3.58	55.28	44.72

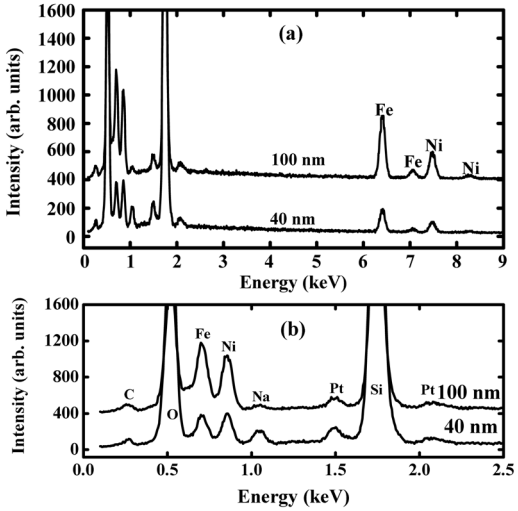

Fig. 2. (a) A representative EDS spectrum observed from the Fe-Ni/Si(111) film of shown thickness for the FG sample. (b)The limit ranges (0~2.5 keV) for the total a energy range is magnified.

Figure 2 gives the representative EDS for the FG samples obtained at two thicknesses. The compositions of the Fe-Ni films deduced from EDS are listed in Table 1. The Pt peaks shown in this spectrum are from the thin layer of platinum coating on the surfaces of the Fe-Ni films, and Si peak is from the substrate. Also, carbon, oxygen, and sodium are shown to contaminate the surface of the films due to expose to air before measurement. As indicated by EDS, the Ni concentration in the $Fe_{1-x}Ni_x$ films is increased by the application of a constant bias magnetic field.

The magnetic hysteresis loops measured with the magnetic field applied parallel to the film plane are presented in Fig. 3(a) for the sample with thickness of 40 nm and Fig. 3(b) for the sample with thickness of 100 nm. The magnetic constants (H_c, M_s, and squarness ratio) obtained using hysteresis loops are summarized in Table 2. Squar-

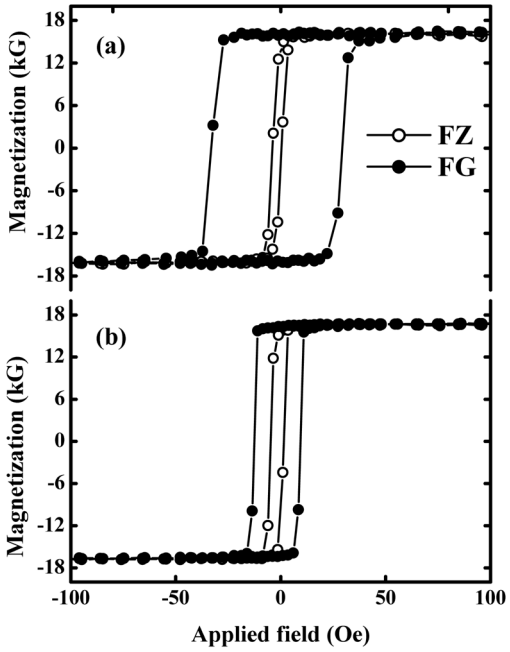

Fig. 3. Magnetic hysteresis loops of Fe-Ni/Si(111) for samples with thickness of (a) 40 nm and (b) 100 nm. Soild and dash lines indicate the "FZ sample" and "FG sample", respectively.

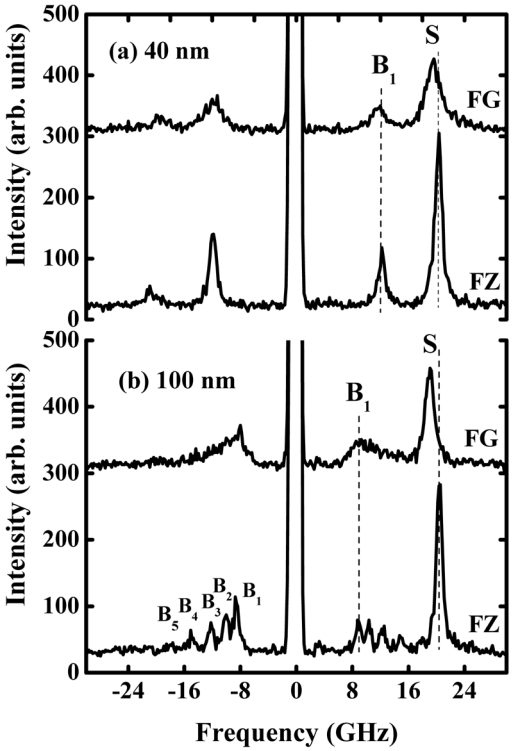

Fig. 4. A typical BLS spectrum for the samples with thickness of (a) 40 nm and (b) 100 nm in the presence of $H = 660$ Oe magnetic field. The peak labeled "B" is the bulk mode and "S" is the surface wave mode. Dash lines indicate the positions of the bulk and surface modes peaks.

ness ratio is found to be about 90% for the FG samples and about 60% for the FZ samples. A squarness ratio nearing 1 for the FG samples indicates that the samples have a preferred orientation in the crystal, or the creation of an induced magnetic anisotropy. The coercivity for the FZ samples has a nearly constant value independent of film thickness and shows good soft magnetic properties. Also the coercivity of the 40 nm FG sample has an anomalously large value ($H_c = 31.3$ Oe) relative to the thicker 100 nm sample. This anomalous phenomenon in the coercivity may be related to the wall type switching such as transition from Bloch to Néel [12, 13].

Figure 4 shows typical BLS spectra for the FZ and FG samples with different thickness (40 and 100 nm) in the presence of H = 660 Oe magnetic field. The peaks labeled B_n ($n = 1$~5) for the FZ sample with thickness of 100 nm are the first- ~ fifth- order bulk SWs. The peaks labeled S is the Damon-Eshach (DE) surface wave. These SW peaks are observed on both frequency sides of the elastic Rayleigh peak centered at zero frequency. In Fig. 4(a) the spectrum for FZ sample with thickness of 40 nm shows the DE peak and first-order bulk peak on the both sides. The weaker DE peak in the Stokes (negative frequency) side is due to the amplitude leakage of the DE mode which is localized on the interface between film and substrate [14]. In Fig. 4(b) the spectrum of the FZ sample with thickness of 100 nm is attributed as the SW due to the DE peak and the weak bulk peaks of $n = 1$~5, where n is the quantum number of the bulk SW. For the FG sample with thickness of 100 nm, the BLS spectrum

Table 2. The magnetization, coercivity, and squarness ratio of hysteresis loops for the samples. And experimental values of magnetic parameters of samples determined by Brillouin scattering.

Sample	Thickness [nm]	VSM			BLS				
		$4\pi M$ [kG]	H_c [Oe]	Squarness Ratio [%]	g	D_B [10^{-9} Oecm^2]	D [meVÅ^2]	$4\pi M_s$ [kG]	$4\pi M_B$ [kG]
FZ	40	16.3	2.12	60.4	1.97	0.79	89.1	15.3	14.8
	100	16.9	3.15	73.5	2.06	0.93	108.7	13.0	12.5
FG	40	16.7	31.26	97.3	2.07	0.78	92.1	14.5	13.9
	100	16.9	11.02	97.5	2.07	1.04	123.9	12.6	12.1

observed only first-order bulk peaks in the both sides and DE peak in the anti-Stokes (high frequency) side. The DE surface wave on the FZ and FG samples with thickness of 100 nm appears only in the anti-Stokes (high frequency) side of the spectrum because of its non-reciprocal nature and the reason that the film is sufficiently so thick that the light cannot interact with the DE mode localized on the lower surface of the film [15]. As shown in Fig. 4, the spectra of DE mode in the FG samples are remarkably broadened with width (full width at half maximum) of about 2.2 GHz, which is much larger than the width of about 1.1 GHz in the FZ samples. It is quite interesting to note that the DE and bulk SW peak widths of the FG samples are comparable to the SW widths of the FZ samples. This is in quite contrast with the very broad SW peaks observed from CoNiPt films prepared by sputtering [16], but the effect of broad SW peaks studied by BLS seems to be related with the grain size.

Figure 5 shows the external field dependence of the Stokes-anti-Stokes intensity ratio (AS/S ratio) of the DE peaks for the film of the thickness of 40 nm. The ratio exhibits a decrease of intensity ratio with increasing external field. Such a tendency may be related to the effect of an applied field [17]. The external field dependence of the intensity ratio is fit to an exponential function of the form

$$\mathrm{AS/S} = I_0 + I_1 \exp(-aH), \tag{1}$$

where I_0, I_1, and a are the best fit constants. Using the experimental formula, the two constants are determined by means of the non-linear least-squares fitting method and the solid line in Fig. 5 is drawn with the best fit values. The best fit values of a are determined to be 0.8 kOe^{-1} and 0.9 kOe^{-1} for the FZ and FG samples, respectively.

To investigate the surface dispersion relation, the spin wave frequency for each mode is measured as a function of the field, as displayed in Fig. 6. Then the frequencies of the DE surface spin wave and bulk spin wave are analyzed using [18, 19]

$$f_{\mathrm{DE}}=\frac{\gamma}{2\pi}[H(H+4\pi M_S)+(2\pi M)^2(1-e^{-2q_{//}d})]^{1/2}, \tag{2}$$

$$f_{\mathrm{bulk}}=\frac{\gamma}{2\pi}[(H+D_B(q_{//}^2+q_{\perp}^2))(H+D_B(q_{//}^2+q_{\perp}^2)+4\pi M_B)]^{1/2}, \tag{3}$$

$$q_{\perp}=\frac{n\pi}{d}$$

where H is the applied magnetic field, γ is the gyromagnetic ratio ($\gamma/2\pi$= 1.4 g [GHz/kOe], g is the spectroscopic splitting factor), d is the thin film thickness, n is the number of order for bulk peaks, $4\pi M_{\mathrm{S}}$ and $4\pi M_{\mathrm{B}}$ are the surface and bulk saturation magnetization, and D_{B} is the SW stiffness constant ([Oecm^2]), which is a measure of intergrain exchange interactions in the film. The D_{B} constant in Eq. (3) is converted into the corresponding D[meVÅ^2] constant by the relation of $D = g\mu_{\mathrm{B}}D_{\mathrm{B}}$ [13]. Here μ_{B} is the Bohr magnetron. Although Eq. (2) is a general expression of the surface magnon frequency, it is an alternative way to determine the surface magnetic constants. The values of exponential term (exp(−2qd)) in

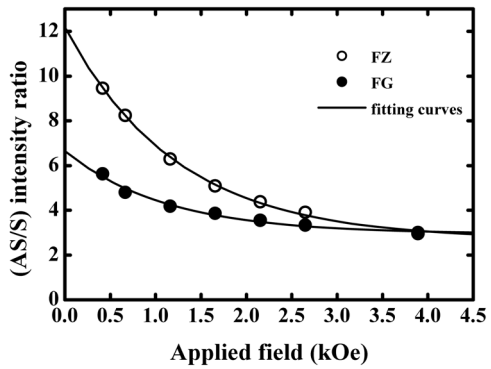

Fig. 5. AS/S intensity ratio as a function of the external field for the FZ and FG samples with thickness of 40 nm. The solid curve is weighted least-squares fit of Eq. (1).

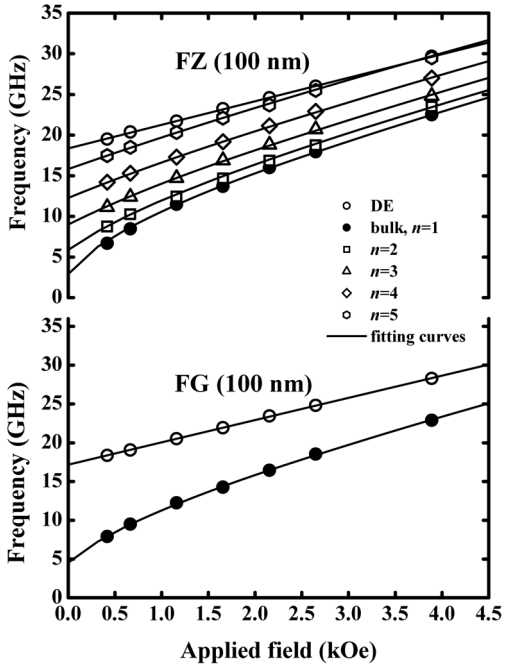

Fig. 6. Variation of spin-wave frequency with applied field for the (a) FZ and (b) FG samples with thickness 0f 100 nm. The symbols are absolute value of the measured frequency shifts for both the Stokes and anti-Stokes data. The solid curves are a weighted least-squares fit of Eq. (2) and Eq. (3).

Eq. (2) is 0.25 and 0.03 for the samples with thickness of 40 and 100 nm, respectively. We are only neglecting the exponential term in Eq. (2) for the samples with thickness of 100 nm because of small contribution on magnetization. Analyzing the data by Eqs. (2) and (3), one can determine the gyromagnetic ratio and surface magnetization by fitting using Eq. (2) and the bulk magnetization and exchange stiffness constant from Eq. (3), respectively. We found that a set of the magnetic parameters which summarized in Table 2, satisfactorily reproduces the surface and bulk dispersion quite well as shown by solid lines in Fig. 6. The bulk magnetizations are, at most, 4%~5% smaller than the surface magnetization. These differences can be regarded as the same with our experimental uncertainty. It indicates a nearly uniform distribution of magnetization across the film. Also the magnetizations determined through BLS have a smaller value than those obtained by VSM data in Table 2. In order to compare the two sets of data, the BLS results have been averaged over the whole film without requiring any knowledge of the sample volume, whereas the VSM measurement accurately requires knowledge of the volume of the magnetic sample. It seems that the obtained magnetizations differ from each other within the experimental uncertainty. The D_B constant of FZ samples has smaller value than that of FG samples. The small D_B values of FZ sample are closely related to the existence of competing ferromagnetic and antiferromagnetic interactions between the nearest neighbor Fe-Fe pairs in the Invar system and the range of exchange interaction between the these pairs [8].

As a possible origin of the difference between FZ and FG samples, we measured the magnetization as a function of the temperature for determination of the SW stiffness constant and the range of exchange interaction. Figure 7

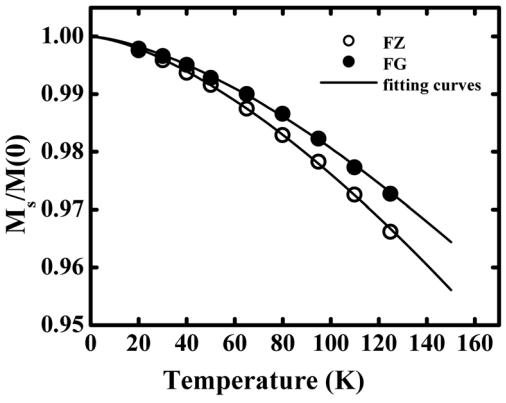

Fig. 7. The temperature dependence of reduced magnetization for the FZ and FG samples with thickness of 40 nm. The solid lines denote the theoretical results using spin-wave theory.

shows the temperature dependence of the magnetization for the 40 nm FZ and FG samples. It is shown that the decrease of magnetization with increasing temperature for the FZ sample is much faster than that for the FG sample. This tendency is well described in terms of the spin-wave approximation as follow equation [20, 21].

$$\frac{M(T)}{M(0)} = 1 - \beta T^{3/2}, \tag{4}$$

where $M(0)$ is the magnetization at 0 K, and β, is best-fit constants. The second term is the familiar Bloch $T^{3/2}$ law.

And to investigate contribution of higher order terms in the magnon dispersion relation, $T^{5/2}$ term is added in Eq. (4). The magnon dispersion relation is given by

$$\frac{M(T)}{M(0)} = 1 - \beta T^{3/2} - \gamma T^{5/2} \tag{5}$$

where γ is best-fit constants. From the fitting result of the experimental data, the values of $M(0)$ and β are determined to be 1472 emu/cm^3 (18.5 kG) and 2.35×10^{-5} K$^{-3/2}$ for the FZ sample and also 1483 emu/cm^3 (18.6 kG) and 1.91×10^{-5} K$^{-3/2}$ for the FG sample, respectively, within the temperature range of 20~100 K using the first and second terms of Eq. (4). The value of g is also determined to be 0.35×10^{-8} K$^{-5/2}$ for the FZ and 0.43×10^{-8} K$^{-5/2}$ for the FG samples within the temperature range of 60~150 K with $M(0)$ and β obtained within the temperature range of 20~100 K. The value of $M(0)$ for the films can be compared with 1420 emu/cm^3 of $Fe_{60}Ni_{40}$ at 4.2 K [22]. By conventional linear spin wave theory, β and γ are also related to the SW stiffness constant D and the average mean square range of exchange interaction through the expressions [20]

$$D = \frac{k}{4\pi}\left(\frac{\varsigma\left(\frac{3}{2}\right) g\mu_B}{M(0)\beta}\right)^{2/3} \tag{5}$$

$$\langle r^r \rangle = \frac{\varsigma\left(\frac{3}{2}\right)}{\varsigma\left(\frac{5}{2}\right)} \frac{16}{3k_B}\left(\frac{\gamma D}{\beta}\right) \tag{6}$$

where $\varsigma\left(\frac{3}{2}\right)$ and $\varsigma\left(\frac{5}{2}\right)$ is the Riemann zeta function, g the spectroscopic splitting factor, μ_B the Bohr magnetron and k_B the Boltzmann constant. The value of g factor was obtained from the BLS experiment. In evaluating the expression of Eq. (5) and Eq. (6) for the temperature regime, we found that the values of the SW stiffness constant D and average mean square range $\langle r^2 \rangle$ is 85.7

meVÅ^2 and 1.53 Å^2 for the FZ sample and 101.6 meVÅ^2 and 2.76 Å^2 for the FG sample, respectively. Values of SW stiffness constant found using the temperature dependence of the magnetization are compared with BLS data in Table 2. The range of exchange interaction (r_{ex}) in unit cell of a_0 can be obtained from the average mean square range of exchange interaction as $\langle r^2 \rangle^{1/2} = r_{ex}\, a_0$ [20]. With the lattice constants from x-ray diffraction we find r_{ex} = 0.4 and 0.8 for the FZ and FG samples with thickness of 40 nm, respectively. This result implies that the range of exchange interaction in the FZ sample is of shorter than that in FG. Considering the difference between the magnetic behaviors of sputtered films with and without bias magnetic field, we believe that sputtering in the magnetic field increased the dimensions of exchange coupling.

4. Conclusion

We have seen the effect on the physical parameters of Fe-Ni films deposited with and without a constant bias magnetic field. The films with a bias field show an increase of grain size, a decrease of lattice constants, and a wall type switching such as a transition from Bloch to Néel. The spin wave spectra for the bias magnetic field samples show increasing linewidth. The spin wave frequencies are measured as a function of the magnetic field up to 4.0 kOe for determination of a set of magnetic constants (g, D, $4\pi M$). The information contributed from exchange interaction in the film allowed us to determine the SW stiffness constant by BLS, and the stiffness constant was compared with the value from magnetization measurement. Furthermore, the SW stiffness constants of the films with a bias magnetic field are larger than those of the films without the field. The difference between the constants implies that the range of exchange interaction in the films with a bias field is longer than that of the films without the field. In the sputtered Fe-Ni films with bias magnetic field, more long-range-ordered clusters with large Fe-Fe separations and ferromagnetic coupling may be present.

References

[1] J. Crangle and G. C. Hallam, Proc. R. Soc. London A **272**, 119 (1963).
[2] E. F. Wassermann, in *Ferromagnetic Materials*, edited by K. H. Buschow and E. P. Wohlfarth (North-Holland, Amsterdam, 1990), Vol. V, p. 240ff.
[3] Y. Ishikawa, S. Onodera and K. Tajima, Solid State Commun. **38**, 561 (1981).
[4] C. A. Bauer and P. E. Wigen, Phys. Rev. B **5**, 4516 (1972).
[5] G. Dumpich, J. Kästner, U. Kirschbaum, H. Mühlbauer, J. Liang, Th. Lübeck, and E. F. WassermannWassermann, Phys. Rev. B **46**, 9258 (1992).
[6] I. Nakai, F. Ono, and O. Yamada, J. Phys. Soc. Jap. **52**, 1791 (1983)
[7] C. A. Bauer and P. E. Wigen, Phys. Rev. B **5**, 4516 (1972).
[8] J. B. Müller and J. Hesse, Z. Phys. B Condens, Mater. **54**, 35 (1984).
[9] J. G. Kim, H. J. Kim, J. Y. Jang, and K. H. Han, J. of Magnetics **9**, 79 (2004).
[10] J. R. Sandercock: in *Light Scattering in Solids III*, ed by M. Cardona and G. Guntherodt (Springer-Verlag, Berlin, 1982) p. 173.
[11] D. Jiles, *Introduction to Magnetism and Magnetic Materials*, 2nd-Edition, Champman & Hall, UK (1998) p.185.
[12] S. Middelhoek, J. Appl. Phys. **34**, 1054 (1961).
[13] J. G. Kim, K. H. Han, S. H. Song, and A. Reilly, Thin Soild Films. **440**, 54 (2003).
[14] A. Yoshihara, H. Sato, J. Mawatari, K. Yoshida, O. Kitakami, and Y. Shimada, J. Magn. Magn. Mater. **221**, 261 (2000).
[15] R. W. Damon, and J. R. Ehbach, J. Phys. Chem. Soilds **19**, 308 (1961).
[16] A. Murayama, M. Miyamura, S. Ishikawa, and Y. Oka, J. Appl. Phys. **67**, 410 (1990).
[17] K. H. Han, J. G. Kim, and S. M. Lee, Solid State Commun. **129**, 261 (2004).
[18] R. E. Camley, J. Magn. Magn. Mater. **200**, 583 (1999).
[19] M. G. Cottam and D. R. Tilley, *Introduction to surface and superlattice excitations*, (Cambridge University Press, New York, 1989), p. 127.
[20] A. K. Majumdar, V. Oestreich, D. Weschenfelder, and F. E. Luborsky, Phys. Rev. B **27**, 5618 (1983).
[21] K. S. Kim, W. N. M, W. Y. Lim, and S. C. Yu, J. of Magnetics **2**, 135 (1997).
[22] R. W. Cochrance and G. M. Graham, Can. J. Phys. **48**, 264 (1970).